

Article

# The Effect of Growth Rate on the Microstructure and Tensile Behaviour of Directionally Solidified Ti-44Al-9Nb-1Cr-0.2W-0.2Y Alloys

Zhu-Hang Jiang, Ning Li, He-Xin Zhang \* and Cheng-Zhi Zhao \*

Key Laboratory of Superlight Materials and Surface Technology of Ministry of Education, College of Materials Science and Chemical Engineering, Harbin Engineering University, Harbin 150001, China; 18686888210@163.com (Z.-H.J.); lining@hrbeu.edu.cn (N.L.)

\* Correspondence: zhanghx@hrbeu.edu.cn (H.-X.Z.); zhaochengzhi@hrbeu.edu.cn (C.-Z.Z.); Tel.: +86-188-4516-5095 (H.-X.Z.); +86-138-9571-8408 (C.-Z.Z.)

Received: 23 June 2018; Accepted: 9 July 2018; Published: 11 July 2018



**Abstract:** Ti-44Al-9Nb-1Cr-0.2W-0.2Y alloys were directionally solidified (DS) at different growth rates varying from 10 to 20  $\mu\text{m/s}$  using a modified liquid metal cooling (LMC) method. The results show that an increase in the growth rate leads to both a decrease in the size of the columnar grains in the directional solidification stable growth zone and a deterioration of the preferred orientation of the  $\alpha_2(\text{Ti}_3\text{Al})/\gamma(\text{TiAl})$  lamellar structure in the columnar grains. The growth direction of the primary dendrite in the quenching zone gradually deflected along the axial direction as the growth rate increased. At the same time, the morphology changed from dendrite to a cystiform dendritic structure, with considerable B2 phase segregation in the dendritic core. Correspondingly, the tensile properties of the alloy decreased at 800 °C with a gradual increase in the cleavage fracture area. These findings show that the low growth rate is beneficial for the preferred orientation and the mechanical properties of the alloy. The content of the B2 phase and the change in the lamellar orientation are the main limiting factors for the tensile properties of the materials at high temperatures.

**Keywords:** Ti-44Al-9Nb-1Cr-0.2W-0.2Y alloy; directional solidification; quenched dendritic; microsegregation; lamellar orientation; 800 °C tensile behavior

## 1. Introduction

TiAl base alloys containing a high Nb content have attracted extensive attention for potential applications in aero engines due to their low density, high specific modulus and creep resistance, as well as their excellent high-temperature properties [1–5]. Amongst the various microstructures of TiAl alloys, the most typical is the fully laminated dual-phased structure that consists of  $\gamma$ -TiAl and  $\alpha_2$ -Ti<sub>3</sub>Al. Fully lamellar TiAl alloys with uniform composition and fine grains have good rupture toughness and strength both at room and at elevated temperatures. Nevertheless, the poor room-temperature ductility, high-temperature resistance and fracture toughness still restrict the applications of these alloys in aerial materials and turbine engines [6,7]. A directional solidification technique can improve the room-temperature ductility of TiAl by obtaining a lamellar orientation that is parallel to the direction of the macroscopic stress or inclined at an angle of less than 45° [8,9].

Numerous methods have been developed to control the orientation of the lamellar structures in directionally solidified (DS) TiAl alloys. These methods all originate from two categories. In the first case, the seed crystals were utilized to induce the inheritance of the newly formed lamellar orientation of the mother column grains [10,11]. In the second case, the solidification path was adjusted so that the  $\beta$  phase preliminarily participates from the liquid. However, when a seeding growth method is employed, it is necessary to ensure that the seed material has good high-temperature stability, and the

growing  $\alpha$ -phase is required to be accurately incorporated into the parent phase during the freezing process. In contrast, it is easier to control the lamellar orientation because  $\beta$  phase precipitation is the only constituent phase of the initial solidification stage.

The elemental composition is the only requirement for a complete  $\beta$  phase transition from the liquid [12]. There are many  $\beta$ -stabilizing elements such as Nb, W, Mo, Cr, Mn and V [13–16]. While ensuring that the alloy solidifies completely along the  $\beta$ -phase path, these stabilizing elements are very likely to cause a certain amount of the B2 phase to remain in the room-temperature tissue. This process is referred to as  $\beta$ -segregation because of the large amount of  $\beta$ -stabilizing elemental segregation in the B2 phase [17,18]. The extreme hardness of the B2 phase is responsible for the ambient temperature brittleness of the  $\beta$  phase TiAl alloy. Due to the extremely high cooling rate,  $\beta$ -segregation is prone to occur during directional solidification. The dendrite growth in the quenched zone shows the initial growth stage of the solidification and may reveal the solidification process of the material at different growth rates. During this period, the analysis of the  $\beta$ -segregation process is very convenient.

Appropriate additions of  $\beta$ -stabilizing elements within a specific range of Al (<49%) can ensure that the material completely solidifies in the  $\beta$  path. However, some  $\beta$ -stabilizing elements, such as W, will greatly increase the nucleation rate during the solidification process, which may lead to difficulties in obtaining columnar crystal growth in the DS TiAl alloy. Therefore, an additional amount of such elements should be strictly limited. As a rare metal, Y may significantly increase the microstructure uniformity and grain boundary strength of the alloys [19]. The simultaneous addition of trace amounts of W and Y may be beneficial for the organization of the materials. At present, there are limited reports about the microstructure of DS TiAl alloys with such a composition.

In this paper, Ti-44Al-9Nb-1Cr-0.2W-0.2Y (at. %) alloys were directionally solidified at varying growth rates and a constant temperature gradient (G) using a modified liquid metal cooling (LMC) method. Optical microscopy (OM, Olympus Inc., Shinjuku District, Tokyo, Japan), scanning electron microscopy (SEM, Carl Zeiss AG, Carl-Zeiss-Straße, Oberkochen, Germany) and other test methods were used to observe the macroscopic and microscopic structures of the DS specimens, especially the dendrite structure in the quenched zone. The effect of the growth rate on the microstructure, especially the lamellar orientation and  $\beta$ -segregation, was intensively investigated. In addition, the role of W and Y microalloying in the material was evaluated.

## 2. Experimental

A master ingot with a nominal composition of Ti-44Al-9Nb-1Cr-0.2W-0.2Y was prepared using Ti (99.7%), Al (99.9%), Nb (99.8%), W (99.9%), Cr (99.9%) and an Al-10 wt. % Y master alloy in a vacuum non-consumable arc-melting furnace with a water-cooled copper crucible and argon protection. In addition, electromagnetic stirring technology was used during the smelting process to ensure the uniformity of the ingot composition. The master batch was processed into a cylinder with a diameter of 10 mm and a length of 100 mm by an electrical discharge machining (EDM) cutting method, and the cylinder was then polished before the directional solidification experiment.

The directional solidification experiment was carried out by applying an improved LMC method. First, a high-purity alumina ceramic (>99.9%) was used as the mold shell material. Second, multi-coil electromagnetic induction heating was used to ensure uniform heating. Third, a graphite insulation sleeve was added between the DS sample and the heating coil to ensure the thermal stability of the heating part. The thermal barrier was used to ensure a high temperature gradient between the sample and liquid metal. The structure of the experimental apparatus is shown in Figure 1. The weight ratio of the Ga-In alloy used in this experiment is 3.72:1. The can loaded with the Ga-In alloy was circulated with cooling water to release heat, and the water temperature was maintained at 20–25 °C. Before the experiment, the pressure in the furnace chamber was lowered to  $5 \times 10^{-3}$  Pa, and the chamber was then filled with argon until the pressure reached 0.5 Pa.

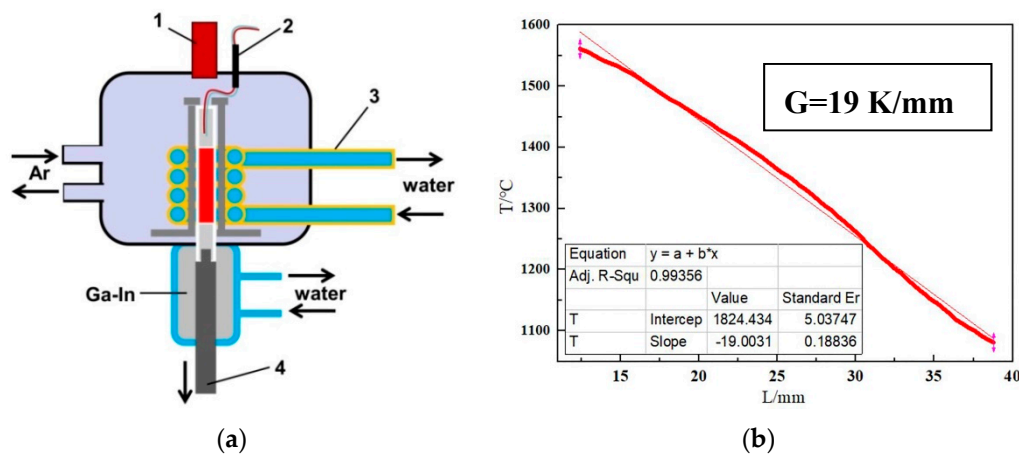


**Figure 1.** (a) Structure of the directional solidification system (1 infrared temperature probe; 2 temperature thermocouple; 3 cooling water and 4 pulling system); (b) Temperature gradient test curve.

W/Re thermocouples and infrared thermometers were used to simultaneously measure the temperature gradients. In Figure 1b, the  $G$  values were approximately equal to 19 K/mm. The directional solidification experiments were performed at a constant electric supply power ( $P$ ) of 5.5 kW and a variable growth rate ( $V$ ) ranging from 10 to 20  $\mu\text{m/s}$ . In this case, the alloy was heated to a temperature of 1750  $^{\circ}\text{C}$  and was stabilized at this temperature for 10 min. To study the solidification process of samples, the specimens with stable growth were quenched to retain the morphology of the primary dendrites.

The metallographic samples of cross-sectional and longitudinal sections of the DS bar were prepared using standard metallographic techniques and were etched in a solution with a composition of 2% $\text{HNO}_3$  + 20% $\text{HF}$  + 78% $\text{H}_2\text{O}$ . The microstructures and the component distributions were examined using an SEM with electron backscattering system equipped with an energy dispersive spectrometer (EDS, Carl Zeiss AG, Carl-Zeiss-Straße, Oberkochen, Germany).

The tensile properties of the ingots were measured by tensile tests at an elevated temperature of 800  $^{\circ}\text{C}$ . The flat tensile specimens were machined using an electro-discharge technique with the tensile axis parallel to the pulling direction of the DS alloys with a stabilized columnar crystal structure. The tensile specimen had a 20 mm gauge length with a 3.5 mm  $\times$  2 mm cross section. All tensile specimens were polished with 2000 grit emery paper and were cleaned using an ultrasonic cleaning machine. Tensile testing was performed at a loading speed of 0.5 mm/min. The fracture surface of the tensile specimens was analyzed by SEM with secondary electron scanning.

### 3. Results and Discussion

#### 3.1. Effect of Growth Rate on Microstructure and Orientation

The directional solidification experiments were carried out on the Ti-44Al-9Nb-1Cr-0.2W-0.2Y alloy in the growth rate range of 10–20  $\mu\text{m/s}$ . The macroscopic structures of the axial section of the DS ingots, which grew a certain distance, are shown in Figure 2a–c. The obvious DS morphologies are evident at the three growth rates, and the relative parameters of the DS sample are shown in Table 1. With an increase in the growth rate, the radial size of the columnar grain decreases. The orientation difference between the long direction of the columnar grains and the axial direction of the ingot also decreases; the preferred orientation of the columnar grain gradually turns from the heat flux direction to the pulling direction. In addition, according to the distribution of the columnar crystals, the main nucleation position of columnar crystal is the inner wall of the mold where cooling occurs preferentially. Both the columnar grain of the posterior nucleation and the previous columnar grain grow in a limited space and gradually reach a steady state. With an increase in the growth rate, the nucleation rate at

the solid-liquid growth interface increases. Thus, the number of columnar grains in the competition grows, and only a few columnar crystals can grow continuously. The orientation difference between the columnar crystal growth direction and the axial direction is small at high speeds; this difference results from the increasing ratio between the pulling rate and the heat dissipation rate. Apparently, the orientation of the columnar grains is more ideal at high growth rates.

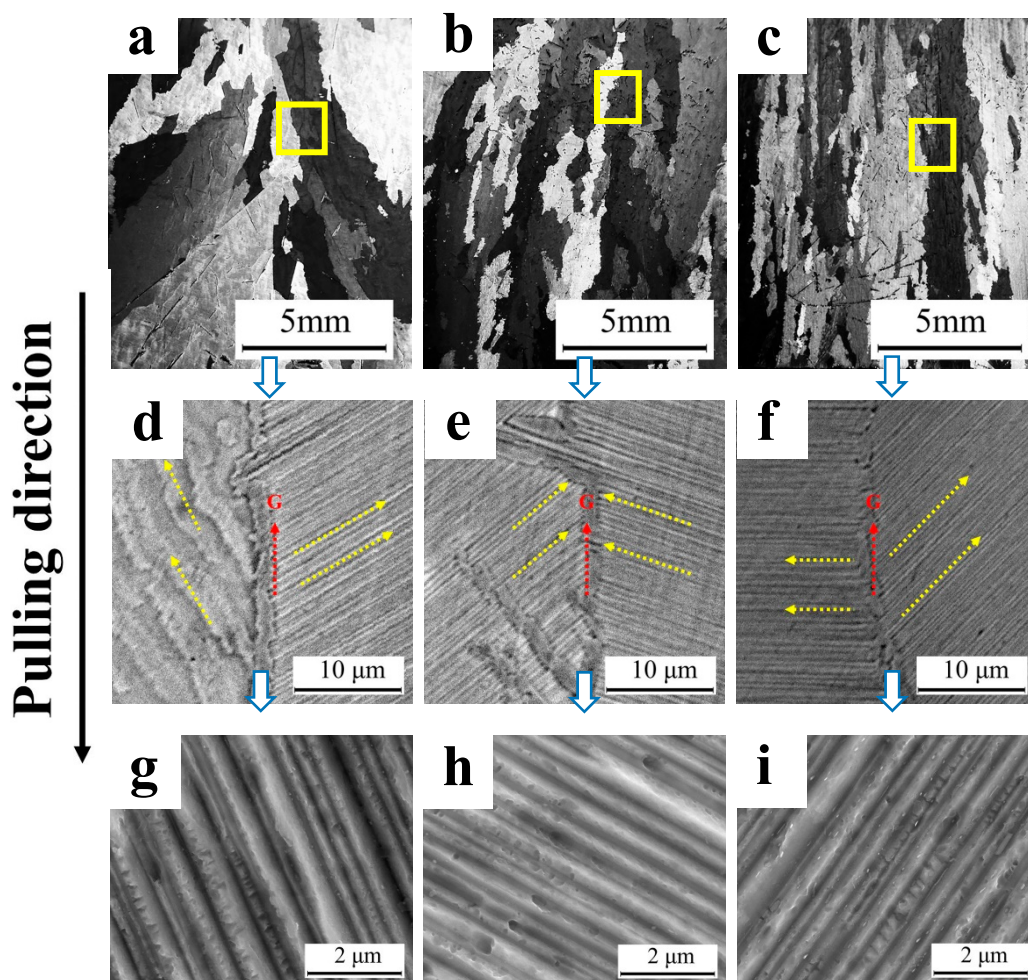


**Figure 2.** Longitudinal macrostructures (a–c) and the corresponding microstructures (d–i) in the stable zone of the DS Ti-44Al-9Nb-1Cr-0.2W-0.2Y (at. %) specimen at growth rates of 10  $\mu\text{m/s}$ , 15  $\mu\text{m/s}$  and 20  $\mu\text{m/s}$ , respectively.

**Table 1.** Morphology parameters of the steadily solidified DS alloys.

Growth Rate	Columnar Grain		Microstructure	
	Radial Size	Lamellar Thickness	Grain Boundary	Misorientation
10 $\mu\text{m/s}$	1.25 mm	150~550 nm	1.8 $\mu\text{m}$	$\beta$ ( $30^\circ + 60^\circ$ )
15 $\mu\text{m/s}$	1 mm	120~600 nm	1.5 $\mu\text{m}$	$\beta$ ( $50^\circ + 70^\circ$ )
20 $\mu\text{m/s}$	0.76 mm	90~670 nm	0.9 $\mu\text{m}$	$\beta$ ( $45^\circ$ ) + $\alpha$ ( $90^\circ$ )

To analyze the relationship between the lamellar orientation and the growth direction of the columnar grain, some typical boundaries of the columnar crystals in the DS alloy were selected and analyzed. The results are shown in Figure 2d–f; high magnification scans of lamellar are shown in Figure 2g–i. The related parameters are listed in Table 1. With an increase in the growth rate, the grain boundary width of the columnar crystal obviously decreased, and the morphology of the grain

boundary became simpler. The wavy lamellar structure formed by the apparent heat flow disturbance at the low growth rate also became straight and stable.

With an increase in the growth rate, the orientation difference between adjacent grain boundaries gradually increases. Moreover, the angle of the columnar grain and its inner lamellar orientation also increase. At a low growth rate, the tissues are all  $\beta$  lamellae with small orientation angles; the orientation angle of the lamellar structure largely turns as the growth rate increases and gradually consists of  $\alpha$  lamellar and large-angle  $\beta$  lamellar phases. This change greatly degrades the preferred orientation of the materials, which may deteriorate the performance of the material. The high multiple scanning observations of the lamellar tissues found that an increase in the growth rate reduces the thickness of the lamellae but decreases the thickness heterogeneity of the lamellar structure. In addition, granular B2 phases are dispersed in the lamellar structure at a high growth rate.

All the results above indicate that the deflection of the columnar crystals to the direction of the heat flow affects the preferred orientation of the lamellar structure. An increase in the growth rate will result in an increase in the slope growth of the non-preferred columnar crystals, and the preferred orientation of the columnar crystal composition can only be obtained at a low growth rate.

### 3.2. Microsegregation and Morphology of the Quenched Dendritic

To analyze the solidification process and the elemental segregation of the DS Ti-44Al-9Nb-1Cr-0.2W-0.2Y alloy at different growth rates, the primary dendrites were obtained by quenching during the stable growth process. The microstructures are shown in Figure 3 (the sampling location of the longitudinal section was at the center of the radius of the specimen); the related parameters are listed in Table 2. The dendrite morphology notably changed with an increase in the growth rate.

In the direction of dendrite growth and at a low growth rate (10  $\mu\text{m/s}$ ), the primary dendrite grows along the direction of the heat flow and is at a  $60^\circ$  orientation with the axial direction of the sample. The direction of the primary dendrite growth is obviously dependent on the axial direction of the material after the drawing rate is increased. This behavior shows that an increase in the growth rate is beneficial for the preferred orientation of the primary grain, which is in accordance with the orientation of the columnar crystal in the stable growth area and shows that the adjustment of the drawing rate can indirectly control the orientation of the columnar crystal. In addition, the dendrite spacing notably decreases, and the integrity of the secondary dendrites decreases gradually. At the same time, the angle between the secondary dendrites and primary dendrites also increases, which led to an increase in the dendrite's aspect ratio.

Regarding the dendrite morphology and composition, the morphology is gradually changed from a dendritic to a cellular dendrite structure with an increase in the growth rate. In addition, the size of the primary dendrite core is significantly increased and the growth of the secondary dendrite core is obviously inhibited by the increase in the primary dendrite density. During the whole transformation process, the microscopic segregation becomes clear. The EDS component analysis of the microstructure of the samples shows that the overall composition of the dendrite is uniform. The composition of the dendrite cores (position 1 and 2 in Figure 3a), which exhibited no clear segregation, is as uniform as that of the overall composition of other dendrites (position 2 in Figure 3b and position 1 and 2 in Figure 3c) and is close to the design components. The dendrite is formed at a high growth rate (position 1 in Figure 3b and position 3 in Figure 3c) is characterized by high segregation, which is the B2 phase, in which the  $\beta$  stable elements such as Nb, Cr and W are enriched. Similar results have also been found in numerous other investigations [12,20]. There is no obvious segregation of the B2 phase when the growth rate is 10  $\mu\text{m/s}$ . However, when  $v = 15 \mu\text{m/s}$ , the strip B2 phase in the core of the primary dendrite and secondary dendrite is evident and is obtained in the contrast between the point scanning and regional scanning of the different parts. When  $v = 20 \mu\text{m/s}$ , the distribution of the B2 phase spread to a wider area in the reticulate distribution. In addition, the Y content in the dendrite gaps is considerably smaller than that in the dendrite core, which indicates that Y promotes nucleation and solid solution strengthening during the solidification process. The residual liquid phase of the dendrite gap during the solidification process lacks

Y. This finding also demonstrates that the Y element optimizes the alloy structure without affecting the grain boundary structure and composition, as has been discussed in Ref. [21].

The above analysis shows that during the directional solidification process of the Ti-44Al-9Nb-1Cr-0.2W-0.2Y alloy, the dendritic stem is the  $\beta$  phase, which indicates that the alloy solidified in the  $\beta$  path. The increase in the growth rate will lead to an incomplete transformation of the high-temperature  $\beta$  phase, which causes an increase in the B2 phase segregation at room temperature, thus leading to the uniformity of the microstructure of the alloy.

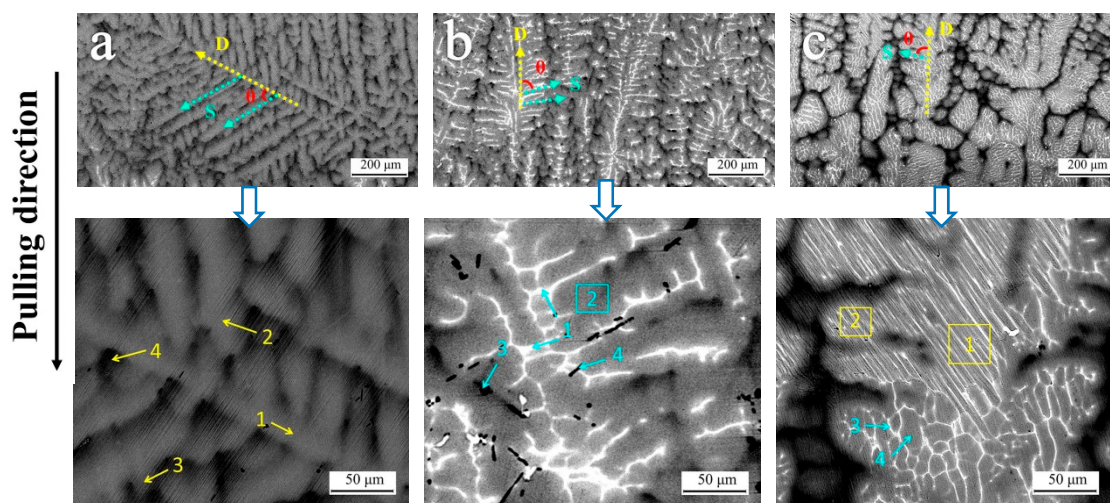


**Figure 3.** Morphologies of the initially solidified dendrite of the quenched zone of the DS Ti-44Al-9Nb-1Cr-0.2W-0.2Y alloy at different growth rates: (a)  $V = 10 \mu\text{m/s}$ ; (b)  $V = 15 \mu\text{m/s}$ ; and (c)  $V = 20 \mu\text{m/s}$  (D: primary dendrite growth direction; S: secondary dendrite growth direction;  $\theta$ : The angle between the primary dendrite and secondary dendrite growth direction).

**Table 2.** Dendritic growth morphology parameters.

Growth Rate ( $v$ )	Primary Dendrite Spacing	Secondary Dendritic Spacing	$\theta$ Angle
$10 \mu\text{m/s}$	$90 \mu\text{m}$	$70 \mu\text{m}$	$60^\circ$
$15 \mu\text{m/s}$	$100\sim 200 \mu\text{m}$	$30 \mu\text{m}$	$>70^\circ$
$20 \mu\text{m/s}$	$200\sim 400 \mu\text{m}$	$20\sim 50 \mu\text{m}$	$>80^\circ$

The X-ray diffraction (XRD) phase and orientation analysis results for the quenched region are presented in Figure 4. The  $\gamma$  phase, the  $\alpha_2$  phase and the B2 phase at three rates are shown, and the different orientation of the  $\gamma$  phase is specially marked. Because the  $\gamma + \alpha_2$  lamellar of the TiAl alloy have a relationship of  $(111) \gamma // (0001) \alpha_2$  [22,23], the lamellar orientation is marked by the  $\gamma$  phase with a square structure, which is easier to analyze.

The main orientations of the  $\gamma$  phase in the alloys at different growth rates are (111) and (202) with a very small amount of (113) and (311) orientations. As the growth rate increases, the (200)– and (002)–oriented  $\gamma$  lamellar increase. There is only a very small amount of the  $\gamma$  phase of the other orientations. The distribution of the B2 phase significantly increases as the growth rate increases. When the growth rate increases to  $20 \text{ m/s}$ , the diffraction peak of the B2 phase is even higher than that of the (111)  $\gamma$  phase. With an increase in the B2 phase, the content of lamellar mass with different orientations increases. Thus, the complexity of the columnar lamellar orientation is improved.

While the columnar crystal size becomes smaller, the volume fraction of the  $\alpha$  grain, in which the lamellar is vertical to the axial direction, obviously increases. This increase has a negative impact on the preferred orientation of the whole material. Therefore, from the perspective of lamellar structure orientation, the low growth rate ( $v = 10 \text{ per m/s}$ ) DS material structure is superior.

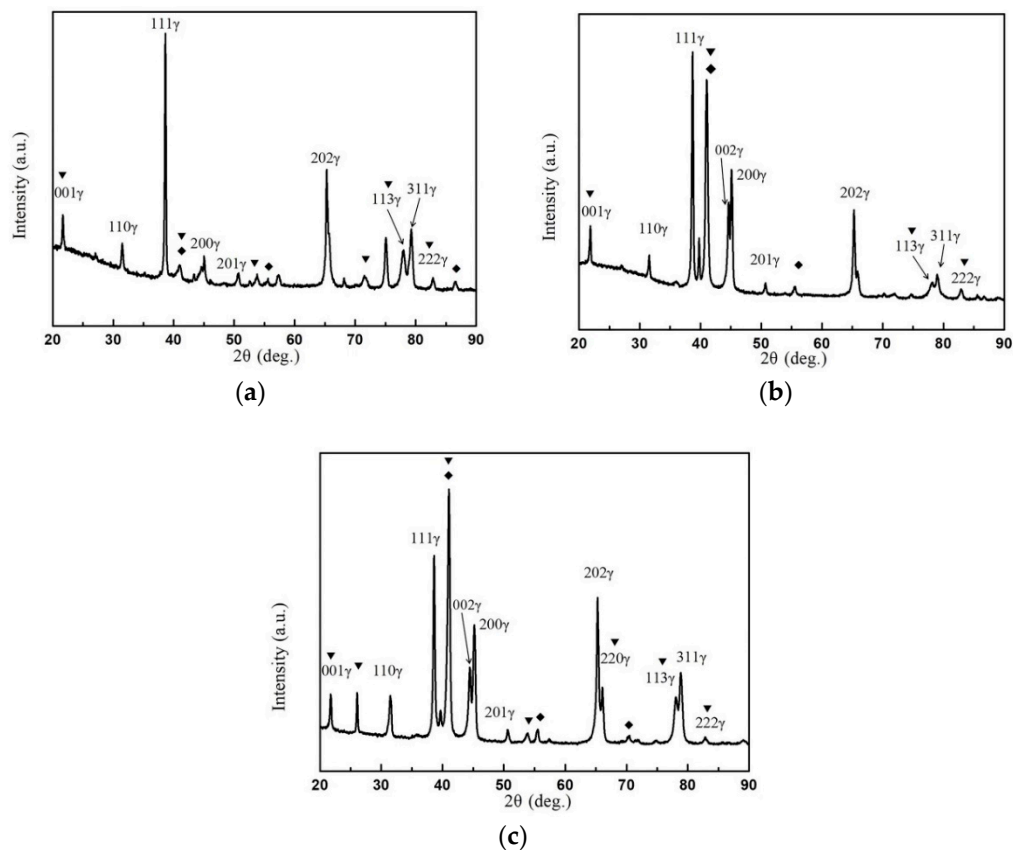


**Figure 4.** X-ray diffraction pattern of the quenched zone of the DS Ti-44Al-9Nb-1Cr-0.2W-0.2Y alloy at different growth rates: (a)  $V = 10 \mu\text{m/s}$ ; (b)  $V = 15 \mu\text{m/s}$ ; and (c)  $V = 20 \mu\text{m/s}$  (▼  $\alpha_2\text{-Ti}_3\text{Al}$  phase, ◆ B2 phase).

### 3.3. Tensile Property Fracture of Directionally Solidified Ti-44Al-9Nb-1Cr-0.2W-0.2Y Alloys

To verify the previous analysis, a tensile test of the alloy was carried out at a rate of 0.5 mm/min at 800 °C. The tensile stress-strain curves and tensile strength histogram are shown in Figure 5. The tensile strength and plastic properties of the specimens obviously decrease, while the growth rate increases, but the elastic modulus of the specimens remains almost unchanged. Interestingly, there is a yield phenomenon of the sample at a growth rate of 10  $\mu\text{m/s}$  before tensile fracture, which suggests an improvement in the toughness of the material. The results conform to the previous analysis of the orientation of the materials and the microsegregation distribution at various growth rates.

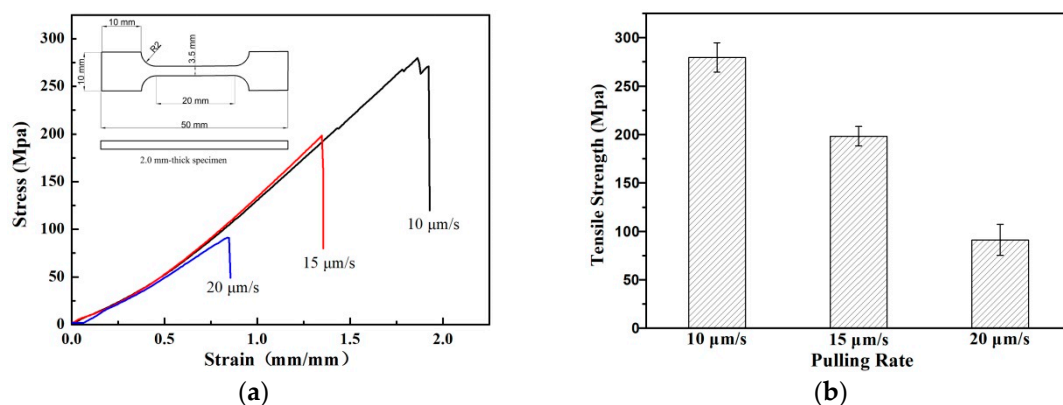


**Figure 5.** (a) Tensile stress and strain curves and (b) tensile strength histogram at 800 °C.

In Figure 6a, the tensile fracture on the fracture surface is dominated by the longitudinal fracture of the small-angle lamellar. The macroscopic morphology of the fracture is extremely uneven. Amongst the longitudinal fractures of the lamellar, there are clear interlamellar fractures that separate the grain from the inside, which indicates that the degree of fracture occurrence is different in the same grain at a high temperature. The heat stress or interlaminar shear force caused by the length difference of the lamellar structure may be the possible reasons. In the latter case, the strain of the lamellae of different lengths is different in the case of the equivalent stress, which will produce a relative displacement, which leads to shear stress generation and causes interlayer cracking. With an increase in the growth rate, the orientation angle of the lamellar structure increases, and the lamella fracture surface with a certain angle appears. In Figure 6b, a small-angle lamellar fracture and a cleavage step exist at the boundary in the multigrain zone. As the lamellae are very thin and the angle of lamellar orientation is not too large, the cleavage steps are rather relaxed. In Figure 6c, the lamellar perpendicular to the tensile direction exists as an obvious interlamellar cleavage surface. The flat cleavage surface and the small-angle lamellar fracture are obviously dissimilar. As opposed to the toughening of the translamellar fracture, the interlamellar fracture usually results in a lower stress intensity factor (K<sub>IC</sub>) value [24]. An increase in these cleavage surfaces is the main reason for a decrease in the tensile properties of the materials.

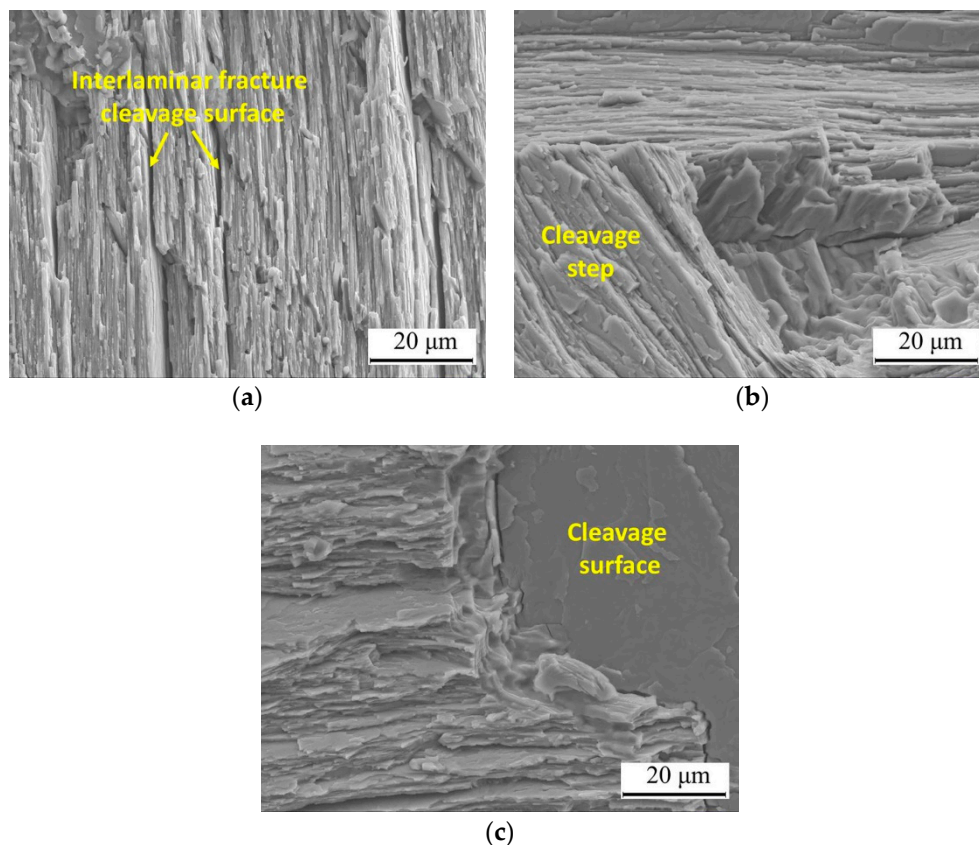


**Figure 6.** Fracture morphology of the tensile test at different growth rates: (a)  $V = 10 \mu\text{m/s}$ ; (b)  $V = 15 \mu\text{m/s}$ ; and (c)  $V = 20 \mu\text{m/s}$ .

The results of tensile tests show that the main cause of the decrease in tensile properties is the deterioration of the lamellar orientation. It is also demonstrated that the tensile properties and plasticity of the lamellar structure with a smaller axial angle are stronger.

In this paper, the lamellar orientation and the  $\beta$ -segregation of the DS Ti-44Al-9Nb-1Cr-0.2W-0.2Y alloy was investigated at different growth rates. The tensile properties at 800 °C were also analyzed.

The application of the modified LMC method achieved a complete DS structure in the range of the changing growth rate. Compared with the higher growth rate, the columnar crystal size of the directional tissue at a low growth rate is larger, and the growth stability is better. Additionally, the lamellar orientation is ideal, and there is no obvious B2 phase segregation, so the overall orientation distribution is uniform and controllable.

The analysis of the small range of the directional solidification growth rate in this paper aims at accurately examining the effect of the growth rate on the lamellar orientation and microsegregation. In addition, the analysis of the elemental distribution of the quenched dendrites also leads to a preliminary understanding the role of W and Y in the microstructural growth during the directional solidification of the TiAl alloy with high Nb content. All these conclusions are helpful references for the elemental design and experimental parameter selection of DS TiAl alloys in the future. Future research directions may include more detailed composition design and better control of the lamellar orientation of the DS TiAl alloys.

#### 4. Conclusions

The microstructural and mechanical properties of Ti-44Al-9Nb-1Cr-0.2W-0.2Y intermetallic DS ingots prepared by a modified LMC method were studied. The following conclusions were reached:

- (1) During the directional solidification process, an increase in the growth rate can refine the size of the columnar grain and grain boundaries, which causes the columnar crystal to be more inclined to axial growth but will reduce the preferred orientation of the columnar lamellar layer and the uniformity of its size and composition.
- (2) As the growth rate increases, the B2 phase segregation in the dendrite is increased, while the growth direction and morphology of the primary dendrites are changed, and the preferred orientation of the lamella is obviously reduced.
- (3) The main factor affecting the tensile properties of the DS Ti-44Al-9Nb-1Cr-0.2W-0.2Y alloy is the angle between the lamellar orientation and the tensile direction. The smaller the angle is, the better the performance. A high growth rate will reduce the preferred orientation of the lamellar structure. A low growth rate is more conducive to obtaining good mechanical properties.

**Author Contributions:** Conceptualization, Z.-H.J.; Methodology, H.-X.Z.; Software, N.L.; Validation, Z.-H.J., N.L. and H.-X.Z.; Formal Analysis, Z.-H.J.; Investigation, Z.-H.J.; Data Curation, H.-X.Z.; Writing-Original Draft Preparation, Z.-H.J.; Writing-Review & Editing, Z.-H.J. and C.-Z.Z.; Project Administration, H.-X.Z.; Funding Acquisition, H.-X.Z.

**Funding:** This research was funded by (Fundamental Research Funds for the Central Universities) grant number (Nos. HEUCFP201719 and HEUCFP201731).

**Acknowledgments:** Thank Fundamental Research Funds for the Central Universities for the grant. Thank a lot for the accompanying of my experimental partners and family. Thanks to the help of the AJE embellishment agency.

**Conflicts of Interest:** The authors declare no conflict of interest.

#### References

1. Appel, F.; Clemens, H.; Fischer, F.D. Modeling concepts for intermetallic titanium aluminides. *Prog. Mater. Sci.* **2016**, *81*, 55–124. [[CrossRef](#)]
2. Ternier, M.; Biamino, S.; Ugues, D.; Sabbadini, S.; Fino, P.; Pavese, M.; Badini, C. Phase transitions assessment on  $\gamma$ -TiAl by Thermo Mechanical Analysis. *Intermetallics* **2013**, *37*, 7–10. [[CrossRef](#)]
3. Kim, S.W.; Na, Y.S.; Yeom, J.T.; Kim, S.E.; Choi, Y.S. An in-situ transmission electron microscopy study on room temperature ductility of TiAl alloys with fully lamellar microstructure. *Mater. Sci. Eng. A* **2014**, *589*, 140–145. [[CrossRef](#)]
4. Ding, X.F.; Lin, J.P.; Zhang, L.Q.; Song, X.P.; Chen, G.L. Microstructures and mechanical properties of directionally solidified Ti-45Al-8Nb-(W, B, Y) alloys. *Mater. Des.* **2011**, *32*, 395–400. [[CrossRef](#)]

5. Loria, E.A. Gamma titanium aluminides as prospective structural materials. *Intermetallics* **2000**, *8*, 1339–1345. [[CrossRef](#)]
6. Tian, S.; Lv, X.; Yu, H.; Wang, Q.; Jiao, Z.; Sun, H. Creep behavior and deformation feature of TiAl-Nb alloy with various states at high temperature. *Mater. Sci. Eng. A* **2016**, *651*, 490–498. [[CrossRef](#)]
7. Inui, H.; Johnson, D.R.; Yamaguchi, M. Directional solidification of TiAl alloys for aligning lamellar microstructures and mechanical properties of directionally-solidified ingots. *Mater. Sci. Forum* **2003**, *426*, 1733–1738. [[CrossRef](#)]
8. Ding, X.; Liao, Y.; Fu, J.; Huang, H.; Liu, W. Analysis of Bootloader and Transplantation of U-Boot Based on S5PC100 Processor. In Proceedings of the Third International Conference on Intelligent Human-Machine Systems and Cybernetics, Hangzhou, China, 26–27 August 2011; pp. 61–64.
9. Jung, I.S.; Jang, H.S.; Oh, M.H.; Lee, J.H.; Wee, D.M. Microstructure control of TiAl alloys containing  $\beta$  stabilizers by directional solidification. *Mater. Sci. Eng. A* **2002**, *329*, 13–18. [[CrossRef](#)]
10. Johnson, D.R.; Masuda, Y.; Inui, H.; Yamaguchi, M. Alignment of the TiAl/Ti<sub>3</sub>Al lamellar microstructure in TiAl alloys by directional solidification. *Mater. Sci. Eng. A* **1997**, *239–240*, 577–583. [[CrossRef](#)]
11. Muto, S.; Yamanaka, T.; Johnson, D.R.; Inui, H.; Yamaguchi, M. Effects of refractory metals on microstructure and mechanical properties of directionally-solidified TiAl alloys. *Mater. Sci. Eng. A* **2002**, *329–331*, 424–429. [[CrossRef](#)]
12. Sun, F.S.; Cao, C.X.; Yan, M.G.; Kim, S.E. Alloying mechanism of beta stabilizers in a TiAl alloy. *Metall. Mater. Trans. A* **2001**, *32*, 1573–1589. [[CrossRef](#)]
13. Chen, G.; Ni, X.; Lin, J.; Wang, J.; Zhang, W.; Xu, J. High temperature intermetallic alloy based on a new intermetallic compound  $\gamma_1$  in the TiAl + Nb system. *Gamma Titan. Aluminides* **2003**, *5*, 153–164.
14. Klein, T.; Schachermayer, M.; Holec, D.; Rashkova, B.; Clemens, H.; Mayer, S. Impact of Mo on the  $\omega_o$  phase in  $\beta$ -solidifying TiAl alloys: An experimental and computational approach. *Intermetallics* **2017**, *85*, 26–33. [[CrossRef](#)]
15. Liu, Z.C.; Lin, J.P.; Wang, Y.L.; Lin, Z.; Chen, G.L.; Chang, K.M. High temperature deformation behaviour of Ascast Ti-46Al-8.5Nb-0.2W alloy. *Mater. Lett.* **2004**, *58*, 948–952. [[CrossRef](#)]
16. Chen, Y.; Niu, H.; Kong, F.; Xiao, S. Microstructure and fracture toughness of a  $\beta$  phase containing TiAl alloy. *Intermetallics* **2011**, *19*, 1405–1410. [[CrossRef](#)]
17. Clemens, H.; Wallgram, W.; Kremmer, S.; Güther, V.; Otto, A.; Bartels, A. Design of Novel  $\beta$ -Solidifying TiAl Alloys with Adjustable  $\beta$ /B2-Phase Fraction and Excellent Hot-Workability. *Adv. Eng. Mater.* **2008**, *10*, 707–713. [[CrossRef](#)]
18. Inkson, B.J.; Clemens, H.; Marien, J.  $\gamma$   $\alpha_2$  B2 Lamellar Domains in Rolled TiAl. *Scr. Mater.* **1998**, *38*, 1377–1382. [[CrossRef](#)]
19. Xu, X.J.; Lin, J.P.; Wang, Y.L.; Gao, J.F.; Lin, Z.; Chen, G.L. Microstructure and tensile properties of as-cast Ti-45Al-(8-9)Nb-(W, B, Y) alloy. *J. Alloys Compd.* **2006**, *414*, 131–136. [[CrossRef](#)]
20. Huang, S.C.; Hall, E.L. The effects of Cr additions to binary TiAl-base alloys. *Metall. Trans. A* **1991**, *22*, 2619–2627. [[CrossRef](#)]
21. Chen, Y.Y.; Li, B.H.; Kong, F.T. Microstructural refinement and mechanical properties of Y-bearing TiAl alloys. *J. Alloys Compd.* **2008**, *457*, 265–269. [[CrossRef](#)]
22. Yamanaka, T.; Johnson, D.R.; Inui, H.; Yamaguchi, M. Directional solidification of TiAl-Re-Si alloys with aligned  $\gamma/\alpha_2$  lamellar microstructures. *Intermetallics* **1999**, *7*, 779–784. [[CrossRef](#)]
23. Fu, H.Z.; Guo, J.J.; Su, Y.Q.; Liu, L.; Xu, D.M.; Li, J.S. Directional solidification and lamellar orientation control of TiAl intermetallics. *Chin. J. Nonferrous Met.* **2003**, *13*, 797.
24. Yu, R.; He, L.L.; Cheng, Z.Y.; Zhu, J.; Ye, H.Q. B2 precipitates and distribution of W in a Ti-47Al-2W-0.5Si alloy. *Intermetallics* **2002**, *10*, 661–665. [[CrossRef](#)]

